Wall depletion length of a channel-confined polymer

Guo Kang Cheong, Xiaolan Li, and Kevin D. Dorfman

Wall depletion length of a channel-confined polymer

Guo Kang Cheong, Xiaolan Li, and Kevin D. Dorfman[*]

Department of Chemical Engineering and Materials Science,

University of Minnesota – Twin Cities,

421 Washington Ave. SE, Minneapolis, MN 55455, USA

Abstract

Numerous experiments have taken advantage of DNA as a model system to test theories for a channel-confined polymer. A tacit assumption in analyzing these data is the existence of a well defined depletion length characterizing DNA-wall interactions such that the experimental system (a polyelectrolyte in a channel with charged walls) can be mapped to the theoretical model (a neutral polymer with hard walls). We test this assumption using pruned-enriched Rosenbluth method (PERM) simulations of a DNA-like semiflexible polymer confined in a tube. The polymer-wall interactions are modeled by augmenting a hard wall interaction with an exponentially decaying, repulsive soft potential. The free energy, mean span, and variance in the mean span obtained in the presence of a soft wall potential are compared to equivalent simulations in the absence of the soft wall potential to determine the depletion length. We find that the mean span and variance about the mean span have the same depletion length for all soft potentials we tested. In contrast, the depletion length for the confinement free energy approaches that for the mean span only when depletion length no longer depends on channel size. The results have implications for the interpretation of DNA confinement experiments under low ionic strengths.

---

[*] dorfman@umn.edu

I. INTRODUCTION

DNA has played a key role in the experimental tests of theories of a polymer confined to a slit [1–14] or a channel [15–27], in particular the models by de Gennes and coworkers for weak confinement [28, 29] and Odijk for strong confinement [30, 31]. The key results of this body of work have been summarized in several recent reviews [32–34]. There are marked advantages to using double-stranded DNA as a model polymer for these experiments: (i) DNA is readily available in monodisperse solutions from biological sources, such as the λ-phage genome; (ii) bright intercalating dyes such as YOYO-1 permit easy imaging of single molecules of DNA by fluorescence microscopy [35]; (iii) the persistence length of DNA, around 50 nm [36], is similar to the length scales available in conventional nanolithography methods; and (iv) DNA can be electrokinetically injected into very small channels, down to 10 nm, through the use of entropy gradients [37, 38]. These advantages must be balanced against the disadvantages arising from DNA's polyelectrolyte nature. In particular, most experiments take place in channels that adopt a (negative) charge at experimentally relevant pH values, while the theories are generally developed for neutral channels. Mapping between experiments and theory thus requires defining a depletion length scale characterizing the "effective channel size" of a neutral system that maps to a particular DNA experiment. In the present contribution, we use a simple model system to test whether a unique depletion length can be defined for the thermodynamics of a channel-confined chain.

The models developed for channel-confined polymers make scaling law predictions for the confinement free energy, $\mathcal{F}$, the average size of the confined chain, $\langle X \rangle$, and the variance about that size, δX^2, for a neutral polymer confined by hard walls [29–31, 39–41]. In some cases, the prefactors for the scaling laws are known exactly [41–43]. These thermodynamic quantities depend on the contour length L of the polymer, its persistence length l_p, the effective width w of the polymer backbone, and the channel size D. The persistence length and effective width of DNA, which are affected by the relative amount of screening of electrostatics by the ionic environment, can be obtained from polyelectrolyte theory [44–47], albeit with some uncertainty arising from the effect of the intercalating dye [48–54]. Intercalation also increases the DNA contour length relative to the rise of naked DNA [55]. However, uncertainties in contour length can be minimized by (i) ensuring uniform staining of the DNA [56] and (ii) using funnel-shaped channels that allow one to interrogate the properties

the same DNA molecule in a range of confinement [18, 22, 23, 25, 57]. For long chains [31], the thermodynamic variables become extensive quantities, so funnel-shaped channels permit a single-molecule test of various scaling laws independent of the contour length.

The situation surrounding the effect of electrostatic interactions on the effective channel size remains unclear. The theories assume a hard wall potential; analyzing experimental data for DNA thus requires defining an effective channel size D_{eff} such that data obtained in a channel of physical size D with charged walls can be mapped to an equivalent neutral channel. In what follows, it proves convenient to recast the problem in terms of a depletion length δ, such that $D_{\text{eff}} = D - \delta$. In an early simulation study, Wang *et al.* [58] observed reasonably good agreement with experimental data [16] by assuming that the wall depletion length is the same as the length scale characterizing segment-segment excluded volume interactions, $\delta = w$. A number of subsequent publications followed this approximation, although it should break down as the channel size decreases [32]. From a practical standpoint, it seems reasonable that the depletion length would be of the same order of magnitude as the DNA effective width, as their electrostatic origins are similar, but should be corrected for the different charge densities of DNA and, say, fused silica [32]. In order to begin reconciling the remaining discrepancies between theory and experiments on DNA, for example in recent work on the extended de Gennes regime [23, 25], it is worthwhile to revisit the concept of a depletion length for a channel-confined polymer.

Our focus here lies in assessing the validity of the depletion length as a way to apply theories for polymers confined by hard walls to confinement in a combination of a hard and soft potential. We thus simulate a model of DNA confined in a tube that confines the polymer with a hard wall and also repels the polymer from the wall by an exponentially decaying, soft potential. While the functional form of this soft potential is similar to the Debye-Hückel formula, the model should not be interpreted as arising from electrostatics. In the electrostatic problem, the key quantity controlling the interactions is the electrostatic screening length due to the ionic strength of the medium, which affects the DNA persistence length, segment-segment interactions, and segment-wall interactions. Moreover, due to the high charge density of DNA, linearized electrostatic models are unlikely to be realistic [47]. By simplifying the problem to a semiflexible chain interacting with a wall through the sum of a hard and soft potential, rather than considering the complexity of the full electrostatic problem, we are able to address the question of the depletion length in a straightforward

3

way.

II.   SIMULATION MODEL AND METHOD

For our simulation model, we adopt the discrete wormlike chain model used in our prior work [58]. The DNA molecule consists of N_b beads with a bond length a. The stiffness of the chain emerges from the bending potential

$$\beta U_{\text{bend}} = \kappa(1 - \cos\theta_i), \tag{1}$$

where θ_i is the angle between a contiguous trio of beads centered on position i and $\beta = (k_B T)^{-1}$ is the inverse Boltzmann factor. The bending constant κ is related to the persistence length by [59]

$$\frac{2l_p}{a} = \frac{\kappa + \kappa\coth(\kappa) - 1}{\kappa - \kappa\coth(\kappa) + 1}. \tag{2}$$

Bead-bead overlap is treated as an infinite energy penalty,

$$\beta U_{\text{ev,bead}} = \begin{cases} \infty, & |r_{ij}| \leq w, \\ 0, & |r_{ij}| > w, \end{cases} \tag{3}$$

where w is the effective width of the beads and r_{ij} is the distance between the center of the beads. Since bond length is smaller than the effective width, $a < w$, we do not enforce the bead-bead excluded volume for contiguous beads [60]. The chain is confined in a circular tube of diameter D. Bead-wall interactions are also treated with an infinite energy penalty similar to Eq. (3) for bead radial positions $r_i \geq (D - w)/2$. For notational purposes, we combine both of these hard core potentials into the quantity U_{ev}, which is infinite if there is bead/bead or bead/wall overlap, and zero otherwise. We also include a soft potential on each bead of the form

$$\beta U_{\text{soft}} = A\exp\left[-\frac{(D/2) - r_i}{\lambda}\right] \tag{4}$$

where A is the dimensionless strength of the potential at the wall surface, and λ is the decay length.

Chain growth simulations in a tube of diameter D were performed with the Pruned-Enriched Rosenbluth Method (PERM) [61, 62], using the modification of our standard code [59, 63] for soft potentials [64]. Briefly, a given tour starts with a bead located at a random

4

radial position within the tube. The weight of the first bead is $W_0 = \exp(-\beta U_{\mathrm{soft}})$. The subsequent beads $n = 1, 2, \ldots$ are placed by first selecting $k = 5$ trial moves from the wormlike chain probability distribution of Eq. (1) and assigning each trial move j an atmosphere

$$a_n^{(j)} = \exp[-\beta(U_{\mathrm{ev}} + U_{\mathrm{soft}})]. \tag{5}$$

In prior work [65], we found that this relatively small value of k is sufficient due to the fine discretization of our model and the stiffness of the wormlike chain model. The Rosenbluth weight for this particular growth step is [61]

$$w_n = \sum_{j=1}^{k} a_n^{(j)}. \tag{6}$$

We then select one trial move with probability

$$p_n^{(j)} = \frac{a_n^{(j)}}{w_n} \tag{7}$$

and update the cumulative Rosenbluth weight of the chain as

$$W_n = w_n W_{n-1}. \tag{8}$$

Within a given tour [61], configurations whose cumulative Rosenbluth weight W_n exceeds an upper bound relative to some target weight are copied (enriched), with each copy assigned half the weight of the original configuration. Conversely, chain growth of configurations whose cumulative Rosenbluth weight falls below some lower bound relative to the target weight is stopped (pruned) to avoid wasting time continuing to grow chains that will make negligible contributions to the ensemble averages. Thus, each tour contributes many configurations to the ensemble through the enrichment process, albeit with some correlations between configurations within a given tour. To set the target weight, we used a bootstrapping method [59] where we first perform "blind" PERM simulations [61] to estimate the target weight, linearly extrapolate from that target weight to the desired long chain length, and then perform "non-blind" PERM simulations [62] using that target weight. Note that any errors in the bootstrapping method affect the efficiency of the simulations, not the accuracy.

A given simulation data set consists of m tours. PERM is effectively a counting method [61], providing an estimate of the partition function. As such, the free energy for an ensemble

of chains of $n+1$ beads is given by

$$\beta F = -\ln\langle W_n\rangle. \tag{9}$$

In the latter, the angular brackets represent the average over all configurations that reach a contour length of $n+1$ beads in any of the m tours. Since the trial moves in our implementation [59, 63] are drawn from the distribution for a wormlike chain, the reference state for the free energy in Eq. (9) is an unconfined, ideal wormlike chain. In order to compute the confinement free energy, we perform a second simulation of a real wormlike chain with the same values of l_p and w as the confined chain but in the absence of confinement. The confinement free energy is then

$$\mathcal{F} = F - F^{\text{free}}, \tag{10}$$

where F^{free} is the result from Eq. (9) for simulations of the unconfined chain. The span of a given configuration is

$$X = \max(x_i) - \min(x_i), \tag{11}$$

with x_i being the axial position of bead $i \in [0, n]$. The mean span of the confined chain is computed by removing the bias in the PERM chain growth,

$$\langle X\rangle = \frac{\langle W_n X\rangle}{\langle W_n\rangle} \tag{12}$$

and the variance in the span is computed in an analogous manner,

$$\delta X^2 = \frac{\langle W_n X^2\rangle}{\langle W_n\rangle} - \langle X\rangle^2. \tag{13}$$

III.   RESULTS

To provide correspondence with typical DNA simulations, we report the results that follow in a dimensional form with a persistence length $l_p = 53$ nm and an effective width $w = 4.6$ nm [58]. The bond length in the simulations is $a = 2.9$ nm; this provides additional resolution of the contour length relative to a touching bead model [60]. The maximum contour length in a given tour is $N_b = 3361$, with the exception of our test of the results as a function of molecular weight, where the maximum contour length is $N_b = 33610$ beads. PERM natively outputs data as a function of molecular weight, and we found that this value of N_b was sufficient to produce extensive scaling for $\mathcal{F}$, $\langle X\rangle$, and δX^2. Each simulation consists of five

6

sets of $m = 10^5$ tours. We estimate the sampling error by treating each set as a separate measurement. The standard errors of the mean for $\mathcal{F}$ and $\langle X \rangle$ are smaller than the size of the data points in all plots. As is the case in prior work [39, 59], the standard error of the mean for δX^2 is somewhat larger, up to 15% of the mean value, and indicated by the error bars in the data that follow.

The simulations provide data in the form $\mathcal{F} = \mathcal{F}(D, A, \lambda; l_p, w, L)$, where A and λ are the strength of the potential and the decay length in Eq. (4). To begin, it proves convenient to consider how data obtained for $A = 0$, corresponding to the hard wall, compare to data at $A = 1$ for different values of λ. Figure 1 presents these data as a map between the hard potential and the soft potential; the abscissa corresponds to the size D used for the simulations in the soft potential for a given value of the decay length λ, and the ordinate is the corresponding effective channel size D_{eff} with $A = 0$ that provides the same value of (a) the confinement free energy, (b) the mean span, and (c) the variance about the mean span. For notational clarity, these effective channel sizes are listed as D_F, D_S and D_V, respectively. The line $D_{\text{eff}} = D$ in Fig. 1 would be the result if the soft potential did not affect the chain thermodynamics. All of the data lie below the line $D_{\text{eff}} = D$, which is to be expected because the soft potential repels the chain from the wall.

As illustrated in the inset of Fig. 2, the depletion length δ is given by the difference between the effective diameter in Fig. 1 and the diameter used for the simulations with the soft potential. For the moment, we will assume that the depletion lengths are different for different thermodynamic quantities and denote them as δ_F, δ_S and δ_V for the confinement free energy, mean span, and variance, respectively. Figure 2 shows the depletion lengths obtained from Fig. 1b for the mean span, δ_S. Similar plots are readily obtained for the other thermodynamic quantities in Fig. 1.

For the shortest decay length in Fig. 2, $\lambda = 5$ nm, we see that the depletion length quickly approaches a constant value as the channel diameter increases. However, for larger values of the decay length λ, larger channel sizes are required until the depletion length reaches its plateau. For the particular simulation data in Fig. 2, the depletion length appears to be reaching a plateau for the largest tube diameters for $\lambda = 10$ nm, while the depletion length continues increasing monotonically for the largest decay length $\lambda = 20$ nm.

The results in Fig. 2 are in qualitative agreement with the rationale provided by Reisner *et al.* for the depletion length for DNA in nanochannels [32]. Explicitly, Reisner *et al.* proposed
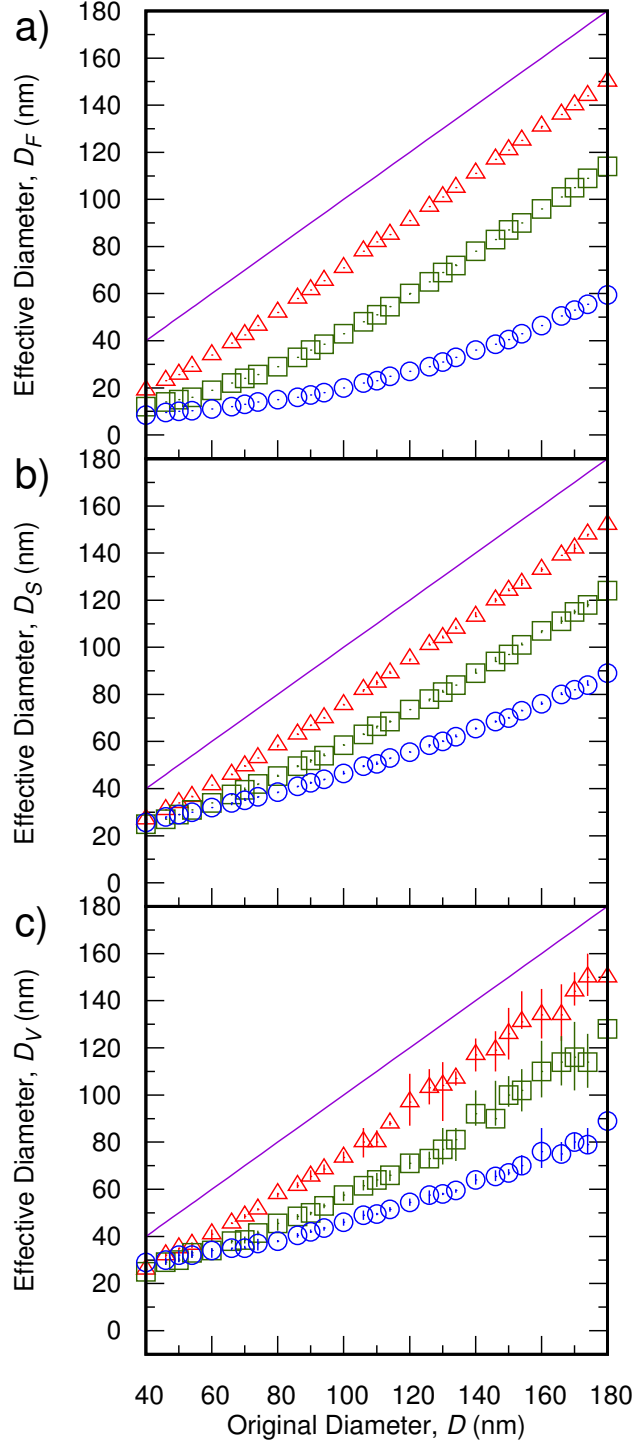
7

FIG. 1. Mapping between simulations with $A = 0$ (hard walls) and $A = 1$ for different values of the decay length λ, where $\triangle$ ($\lambda = 5$ nm) $\square$ ($\lambda = 10$ nm) $\bigcirc$ ($\lambda = 20$ nm). The effective channel sizes D_F, D_S, and D_V are the sizes of the channels with $A = 0$ that have the same value of the confinement free energy, span, and variance, respectively, as the channel with $A = 1$. The solid line in each panel would be the result if the soft potential had no effect on the thermodynamics. Error bars represent the standard error of the mean.
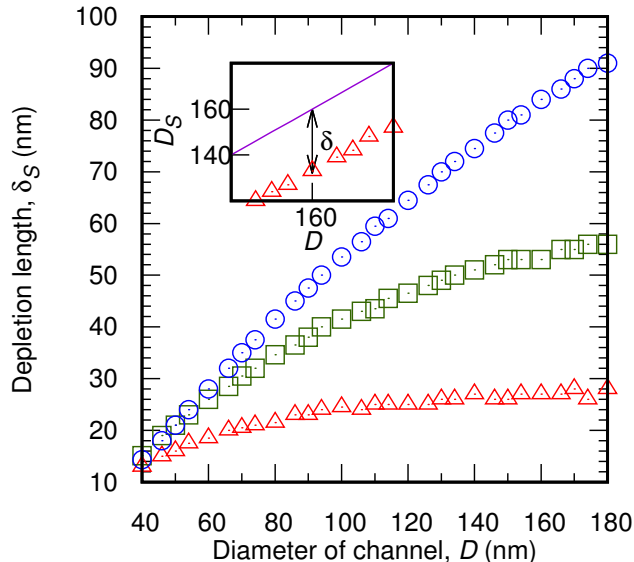
FIG. 2. Depletion length for the mean span, δ_S, obtained from the data in Fig. 1b. The data correspond to $A = 1$ for different values of the decay length λ, where $\triangle$ ($\lambda = 5$ nm) $\square$ ($\lambda =10$ nm) $\bigcirc$ ($\lambda = 20$ nm). The inset illustrates how the depletion length is computed from the effective diameter for the mean span.

that the depletion length could be computed in a manner analogous to the Stigter effective width [47] by considering a rod interacting with a charged surface. Importantly, they point out that this model should break down when the channel size decreases such that the double layers from surfaces on opposite sides of the channel overlap. This is essentially the behavior exhibited in Fig. 2, albeit for a simpler physical system; if the tube is sufficiently large, the depletion length becomes a constant.

The key question in our work is whether there is a unique depletion length, δ, describing the thermodynamics of a confined chain. The data in Fig. 3 indicate that this is not the case. For all channel sizes, we find that the ratio of depletion lengths δ_V/δ_S in Fig. 3a is unity to within the sampling error. In contrast, we only find that the ratio of depletion lengths δ_F/δ_S in Fig. 3b becomes unity when the depletion length has become independent of the channel size. In order to show this behavior, we increased the maximum diameter for all three data sets beyond those of Fig. 1, up to $D = 360$ nm for the $\lambda = 20$ nm case. The error bars were obtained by propagating from the errors in depletion length of variance and the errors in depletion length of span, assuming zero covariance since the mappings were done separately.
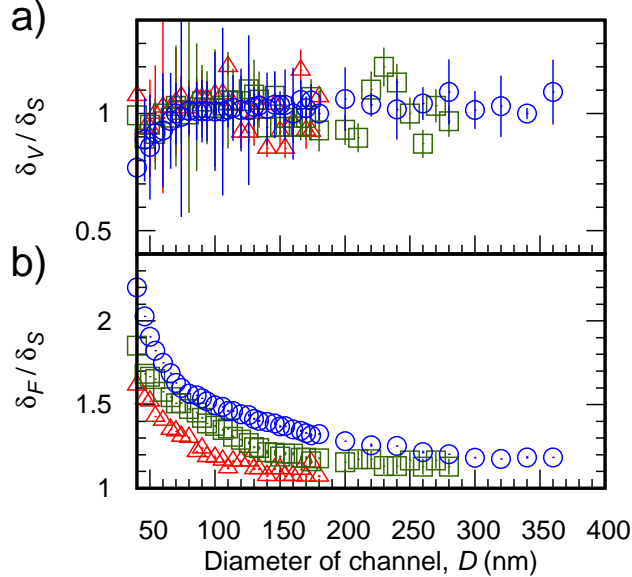
9

FIG. 3. Ratio of the depletion length from mapping free energy, δ_F and variance, δ_V, relative to the depletion length for the mean span, δ_S, for $A = 1$ and different decay length, λ, where $\triangle$ ($\lambda =$ 5 nm) $\square$ ($\lambda =$10 nm) $\bigcirc$ ($\lambda = 20$ nm).

Inasmuch as our physical system is considerably simpler than the DNA-fused silica system used in experiments, we can go further in quantifying the criteria necessary for the depletion length to become independent of channel size. Let us denote the value of the soft potential in Eq. (4) at the channel center as

$$A_0 = A \exp\left(-\frac{D}{2\lambda}\right) \tag{14}$$

Figure 4 plots the magnitude of the depletion length as a function of the the potential at the center of the channel, A_0. To compress the data, we chose to normalize the depletion length with the decay length; we would not expect collapse of the data using this normalization because the depletion length must depend on both the magnitude of the potential at the channel wall (A) and the rate of decay (λ). In addition to the data already presented in Fig. 3, we performed additional simulations at $A = 2$ and $A = 1/2$ for an intermediate value of the decay length, $\lambda = 7$ nm, to provide almost eight decades of data for A_0. Overall, we find that the depletion lengths δ reach a constant value for $A_0 \lesssim 10^{-5}$. We chose a conservative value of 10^{-5} here, keeping in mind that this value is within any practically relevant margin of error arising from uncertainties in the physical parameters in experiments.

The value of $A_0 = 10^{-5}$ as the value where depletion length become insensitive to A_0 was

10

also tested for higher molecular weight. This is presented as the second column to Figure 4. The value $A_0 = 10^{-5}$ remains robust up to our maximum value of $N_b = 33610$ beads, an order of magnitude larger. Due to the massive increase in molecular weight, the standard error for variance about mean span increases to up to 36% of the mean value. However, the perfect collapse in the data for depletion length from free energy and span is a strong indicator for the robustness.

The key result of our analysis is that this value of the potential at the center line, $A_0 \lesssim 10^{-5}$, corresponds to the point at which double layer overlap no longer makes a significant contribution to the confinement thermodynamics. Indeed, by recasting the abscissa of Fig. 3 in terms of the potential strength measured at the tube center, we see a qualitative agreement for the ratio of depletion length for the mean span and the confinement free energy for all thermodynamic properties for values of $A_0 \lesssim 10^{-5}$ in Fig. 5, independent of the particular value of A or λ.

IV. DISCUSSION

While the exact origin of the discrepancy between different depletion lengths is difficult to explain beyond a phenomenological description of the simulation results and the heuristic that the soft potential should be weak enough at the bulk center of the channel, the results we have obtained nonetheless have important implications for analyzing DNA confinement experiments. In most cases, experiments compare the mean span and/or the variance obtained in experiments to theory or simulation, for example our recent work using confinement spectroscopy [22, 23]. In these cases, the question of the exact value of the depletion length remains an open question for quantitative comparisons [22, 23]. However, we cannot ascribe any discrepancy between the experiments and theory (or simulations) to a possible problem with the concept of a depletion length — even if there is double-layer overlap in the experimental system. In the analysis of these experiments, we could treat the depletion length as an adjustable parameter for, say, comparing the experimental results for the mean span to simulations. Once the best-fit depletion length is established from the measurements of the mean span, it is no longer an adjustable parameter when analyzing the variance. As such, we view our results for the depletion length of the mean span and variance as support for previous analyses of experimental data.
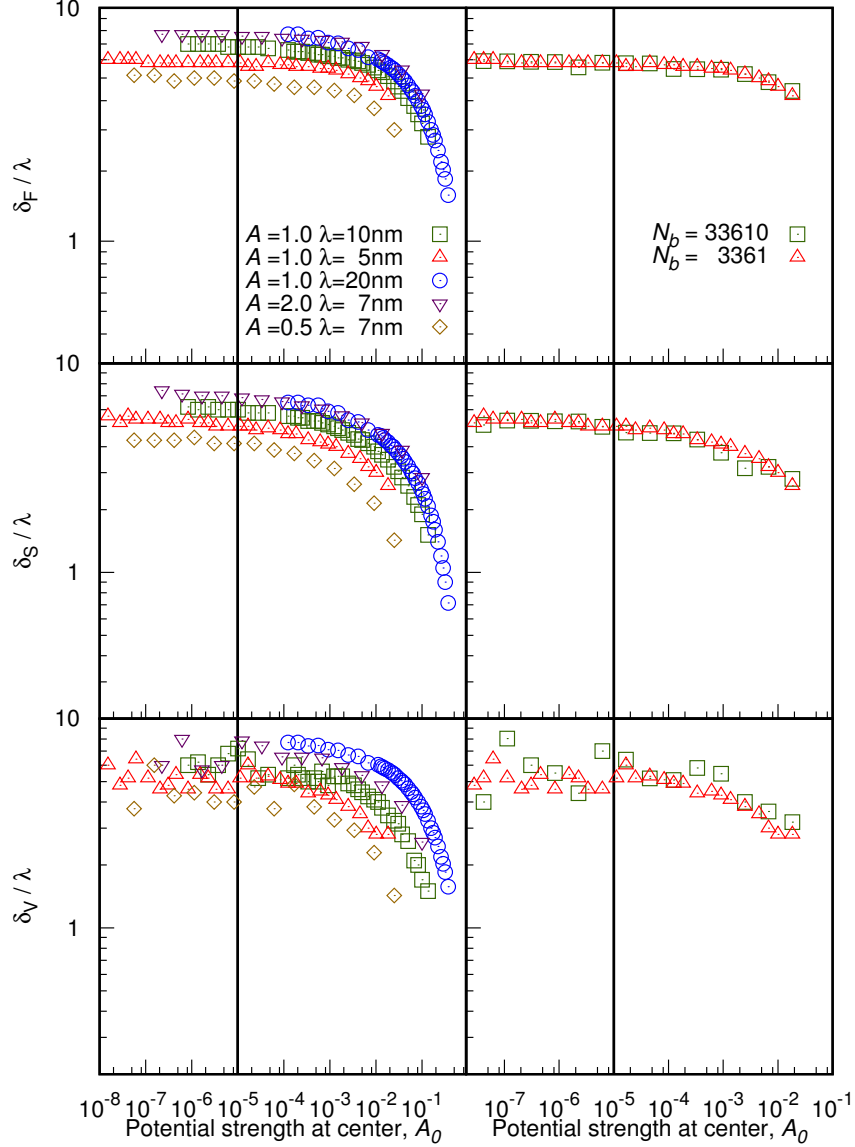
FIG. 4. Normalized depletion length, δ/λ versus potential strength at center, A_0 for different potential strengths at the wall, A, and different decay lengths, λ. The vertical line indicates $A_0 = 10^{-5}$, where the depletion lengths become insensitive to A_0. The first column corresponds to data for $N_b = 3361$ for the various combinations of A and λ. The second column corresponds to the test for high molecular weight for $A = 1.0$ and $\lambda = 5$ nm.

The situation becomes more complicated when DNA confinement is used to measure the confinement free energy [14]. Our results suggest that these experiments should be conducted in high ionic strength buffers such that the Debye length is small compared to the confinement length scale. This is indeed the case in previous experiments [14].
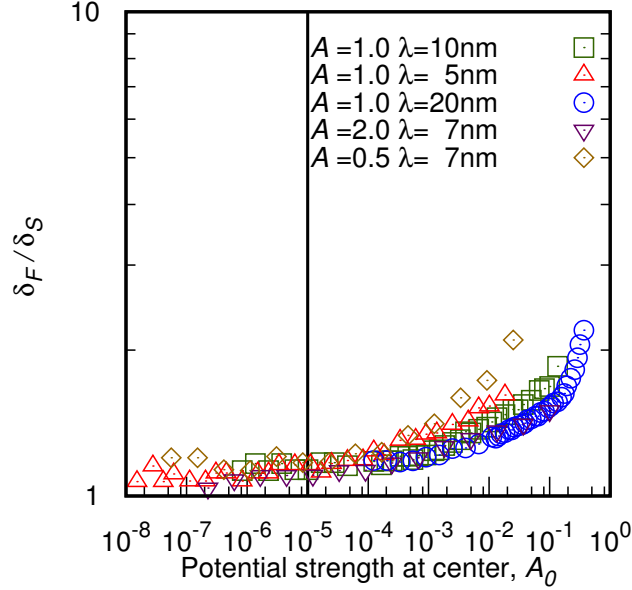
FIG. 5. Ratio of the depletion length from mapping the confinement free energy, δ_F, and mean span, δ_S, versus potential strength at center, A_0 for different potential strengths at the wall, A, and different decay lengths, λ. The vertical line indicates $A_0 = 10^{-5}$.

It is worthwhile to see how our results translate into relevant experimental systems for DNA. If we postulate that the criterion from our simulations, namely that the wall potential at the center of the channel should decay to $10^{-5}k_{\mathrm{B}}T$, applies to the full electrostatic problem as well, we can determine when double-layer overlap is a potential problem. For these calculations, we considered TBE buffer, which is commonly used in experiments, and determined the ionic concentration of the system through an iterative procedure of solving the system chemical equilibria [66]. We have also included in our calculation the presence of 0.5% (v/v) β-mercaptoethanol (BME) which is commonly present in DNA confinement experiments to delay the onset of photobleaching [6]. To model the zeta potential of the channel walls, which are typically fused silica or PDMS, we used the phenomenological approximations proposed by Kirby and Hasselbrink [67],

$$\frac{\zeta_{\text{silica}}}{\text{pC}}[\text{mV}] = 2 + 7(\text{pH} - 3) \tag{15}$$

$$\frac{\zeta_{\text{PDMS}}}{\text{pC}}[\text{mV}] = 5.27 - 4.67(\text{pH}) \tag{16}$$

where pC is the negative base 10 logarithm of ion concentration, analogous to the definition
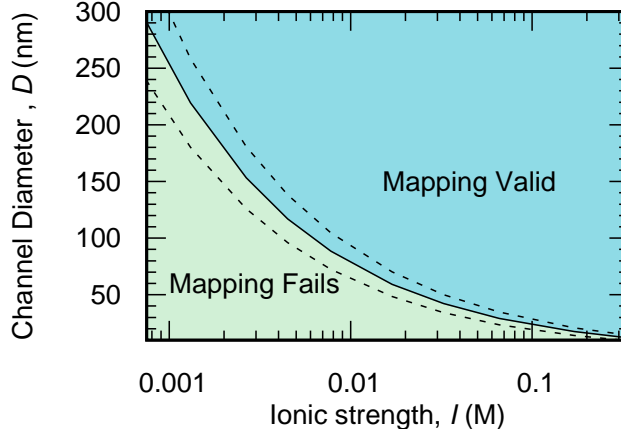
FIG. 6. Phase diagram for the double layer overlap as a function of channel diameter, D, and the ionic strength of buffer, I, for fused silica channels. The onset of double layer overlap is the region labeled as "Mapping Fails" while the region where double layer overlap disappears is labeled as "Mapping Valid". The upper and lower limits indicated by the broken lines represent the results when $A_0 = 10^{-6}$ and $A_0 = 10^{-4}$ are used, respectively.

of pH. For completeness, we have set the Bjerrum length,

$$l_B = \frac{e^2}{4\pi\epsilon_b\epsilon_0 k_{\mathrm{B}}T} \tag{17}$$

to be the representative length scale of the double layer, following the suggestion by Viovy [68]. The sum of the double layer length scale and the distance needed for the zeta potential to decay to $10^{-5}k_{\mathrm{B}}T$ sets the minimum radius needed for the channel size such that the mapping to a hard wall theory works.

Our results in Fig. 6 indicate that at a relatively common experimentation concentration of 1x TBE for fused silica channels, dimensions smaller than 40 nm should encounter double layer overlap effects. We found that the phase diagram for PDMS channel is only marginally different from that of the silica channel. We have also looked at the results if a more conservative value of $A_0 = 10^{-6}$ or a less conservative value of $A_0 = 10^{-4}$ is chosen instead. The region not bounded by the two broken lines of Fig. 6 is where we are most confident about our result. While this is a good guide to experimental studies, we realize that the electrostatic potential within the channel is usually not of the form shown in Eq. (4) especially in the region where the ionic strength is very small [69].

Going forward, it is important to be sure that the condition embodied in Fig. 6 is met if the experimental data are to be compared to theory. For example, working at very low ionic

14

strengths [4, 13, 19] is a facile strategy to increase DNA stretching through a combination of electrostatic repulsion from the walls (which reduces the effective channel size) and the increased persistence length of the DNA backbone [44–46]. In such experiments, it may prove more challenging to match the experimental data to theories for neutral polymers because the DNA-wall electrostatic interactions are sensible throughout most of the channel cross-section.

While we have focused here on the concept of a depletion length, our toy model is not sufficient to say anything meaningful about the magnitude of the depletion length for DNA confined in typical channel materials like fused silica. This is not a trivial calculation. The Onsager-like calculation proposed by Reisner *et al.* [32] is a useful starting point, and likely to be a sufficient improvement over simply using the DNA effective width for cases where the Debye length is small compared to the channel width. When electrostatic interactions with the wall extend over longer distances in the channel, this model is not appropriate [32]. To date, simulations that attempt to consider electrostatic interactions between DNA and charged walls do so at the mean-field, Debye-Hückel level [70, 71]. DNA is a highly charged polyelectrolyte, so it is not clear that Debye-Hückel results will prove to be a meaningful model for DNA confinement. Indeed, the Stigter model uses the Guoy-Chapman model, and it may prove that ion-ion correlations that are not included in a mean-field model are important for the DNA-wall interactions.

One possible approach to model DNA-wall interactions for the case where the Debye length is a substantial fraction of the channel cross section is a self-consistent solution for the electrostatic interactions, where the configuration of the DNA and the ion distribution are determined simultaneously to account for the perturbation to the ion distribution near the walls by the presence of the DNA. Including such interactions entail a substantial increase in the computational costs of the model, but may be necessary if one desires a quantitatively accurate model of the DNA-wall interactions. However, such a model would still neglect the effect of other additives in the buffer besides the salt. For example, most experiments use a polymer in the buffer (e.g., polyvinylpyrrolidone) to suppress electroosmotic flow and to minimize DNA-wall adsorption to defects in the channel. Experiments in very narrow slits suggest that the DNA-polymer interactions have a non-trivial effect on the DNA mobility [72].

V. CONCLUDING REMARKS

In the present contribution, we used a relatively simple model of a self-avoiding, wormlike chain confined to a hard tube with an additional soft, repulsive potential to test the frequently used assumption of a depletion length to map experiments using channel-confined DNA to a neutral chain model. This choice of model system allowed us to examine this question without additional complications related to the long-range electrostatics and ion-ion correlations that are present in the experimental system. Our simulations indicate that the concept of a depletion length is well defined for the size metrics, independent of the magnitude or decay length of the soft potential. However, we only found congruence between the depletion length for the confinement free energy and the size metrics in the case where the soft potential reaches a low enough strength at the center of the channel, approximately $10^{-5}k_BT$. Fortunately, for most experimental systems, the Debye length is small compared to the channel cross section and the surface potential of the walls is not too high, so this condition is met. However, there is a small body of experimental data [4, 13, 19] that uses low ionic strength buffers where the Debye lengths are a substantial fraction of the channel. It is also possible (albeit challenging) to operate with silica-based nanochannels that are below 20 nm in cross-section [37, 38, 73], where even high ionic strength buffers produce Debye lengths that have non-trivial extents.

While we have been somewhat critical about the interpretation of DNA-based experiments to test models for channel-confined polymers, our analysis does not dampen our overall enthusiasm towards this model experimental system. Although there are challenges in using DNA beyond those discussed here, for example the inability to tune the system so that different confinement regimes span multiple decades in channel size [39, 74], DNA remains the most convenient model system for studying confined polymers. While it may ultimately prove challenging to use DNA to test the existing models down to the prefactors for the scaling laws [23, 25, 41–43], there is no better experimental system to directly visualize the effects of confinement at the single molecule level and investigate the universal properties of confined polymers at the scaling level.

16

ACKNOWLEDGMENTS

---

[1] Y.-L. Chen, M. D. Graham, J. J. de Pablo, G. C. Randall, M. Gupta, and P. S. Doyle, Phys. Rev. E **70**, 060901 (2004).

[2] A. Balducci, P. Mao, J. Han, and P. S. Doyle, Macromolecules **39**, 6273 (2006).

[3] A. Balducci, C.-C. Hsieh, and P. S. Doyle, Phys. Rev. Lett. **99**, 238102 (2007).

[4] K. Jo, D. M. Dhingra, T. Odijk, J. J. de Pablo, M. D. Graham, R. Runnheim, D. Forrest, and D. C. Schwartz, Proc. Natl. Acad. Sci. USA **104**, 2673 (2007).

[5] D. J. Bonthuis, C. Meyer, D. Stein, and C. Dekker, Phys. Rev. Lett. **101**, 108303 (2008).

[6] C. C. Hsieh, A. Balducci, and P. S. Doyle, Nano Lett. **8**, 1683 (2008).

[7] E. A. Strychalski, S. L. Levy, and H. G. Craighead, Macromolecules **41**, 7716 (2008).

[8] J. Tang, S. L. Levy, D. W. Trahan, J. J. Jones, H. G. Craighead, and P. S. Doyle, Macromolecules **43**, 7368 (2010).

[9] P. K. Lin, C. C. Hsieh, Y. L. Chen, and C. F. Chou, Macromolecules **45**, 2920 (2012).

[10] E. A. Strychalski, J. Geist, M. Gaitan, and L. E. Locascio, Macromolecules **45**, 1602 (2012).

[11] L. Dai, D. R. Tree, J. R. C. van der Maarel, K. D. Dorfman, and P. S. Doyle, Phys. Rev. Lett. **110**, 168105 (2013).

[12] J. J. Jones, J. R. C. van der Maarel, and P. S. Doyle, Phys. Rev. Lett. **110**, 068101 (2013).

[13] J. Lee, S. Kim, H. Jeong, G. Y. Jung, R. Chang, Y.-L. Chen, and K. Jo, ACS Macro Lett. **3**, 926 (2014).

[14] A. R. Klotz, L. Duong, M. Mamaev, H. W. de Haan, J. Z. Y. Chen, and W. W. Reisner, Macromolecules **48**, 5028 (2015).

[15] J. O. Tegenfeldt, C. Prinz, H. Cao, S. Chou, W. W. Reisner, R. Riehn, Y. M. Wang, E. C. Cox, J. C. Sturm, P. Silberzan, and R. H. Austin, Proc. Natl. Acad. Sci. USA **101**, 10979 (2004).

[16] W. Reisner, K. J. Morton, R. Riehn, Y. M. Wang, Z. Yu, M. Rosen, J. C. Sturm, S. Y. Chou,

E. Frey, and R. H. Austin, Phys. Rev. Lett. **94**, 196101 (2005).

[17] W. Reisner, J. P. Beech, N. B. Larsen, H. Flyvbjerg, A. Kristensen, and J. O. Tegenfeldt, Phys. Rev. Lett. **99**, 058302 (2007).

[18] F. Persson, P. Utko, W. Reisner, N. B. Larsen, and A. Kristensen, Nano Lett. **9**, 1382 (2009).

[19] Y. Kim, K. S. Kim, K. L. Kounovsky, R. Chang, G. Y. Jung, J. J. DePablo, K. Jo, and D. C. Schwartz, Lab Chip **11**, 1721 (2011).

[20] A. Karpusenko, J. H. Carpenter, C. Zhou, S. F. Lim, J. Pan, and R. Riehn, J. Appl. Phys. **111**, 024701 (2012).

[21] K. L. Kounovsky-Shafer, J. P. Herna, K. Jo, T. Odijk, J. J. D. Pablo, and D. C. Schwartz, Macromolecules **46**, 8356 (2013).

[22] D. Gupta, J. Sheats, A. Muralidhar, J. J. Miller, D. E. Huang, S. Mahshid, K. D. Dorfman, and W. Reisner, J. Chem. Phys. **140**, 214901 (2014).

[23] D. Gupta, J. J. Miller, A. Muralidhar, S. Mahshid, W. Reisner, and K. D. Dorfman, ACS Macro Lett. **4**, 759 (2015).

[24] M. Alizadehheidari, E. Werner, C. Noble, M. Reiter-Schad, L. K. Nyberg, J. Fritzsche, B. Mehlig, J. O. Tegenfeldt, T. Ambjornsson, F. Persson, and F. Westerlund, Macromolecules **48**, 871 (2015).

[25] V. Iarko, E. Werner, L. K. Nyberg, V. Müller, J. Fritzsche, T. Ambjörnsson, J. P. Beech, J. O. Tegenfeldt, K. Mehlig, F. Westerlund, and B. Mehlig, Phys. Rev. E **92**, 062701 (2015).

[26] W. F. Reinhart, J. G. Reifenberger, D. Gupta, A. Muralidhar, J. Sheats, H. Cao, and K. D. Dorfman, J. Chem. Phys. **142**, 064902 (2015).

[27] J. Sheats, J. G. Reifenberger, H. Cao, and K. D. Dorfman, Biomicrofluidics **9**, 064119 (2015).

[28] F. Brochard and P. G. de Gennes, J. Chem. Phys. **67**, 52 (1977).

[29] M. Daoud and P. De Gennes, J. Phys. **38**, 85 (1977).

[30] T. Odijk, Macromolecules **1344**, 1340 (1983).

[31] T. Odijk, Phys. Rev. E **77**, 060901(R) (2008).

[32] W. Reisner, J. N. Pedersen, and R. H. Austin, Rep. Prog. Phys. **75**, 106601 (2012).

[33] K. D. Dorfman, S. B. King, D. W. Olson, J. D. P. Thomas, and D. R. Tree, Chem. Rev. **113**, 2584 (2013).

[34] L. Dai, C. B. Renner, and P. S. Doyle, Adv. Colloid Interface Sci. **232**, 80 (2015).

[35] S. Gurrieri, K. S. Wells, I. D. Johnson, and C. Bustamante, Anal. Biochem. **249**, 44 (1997).

[36] C. Bustamante, J. F. Marko, E. D. Siggia, and S. Smith, Science **265**, 1599 (1994).

[37] H. Cao, J. O. Tegenfeldt, R. H. Austin, and S. Y. Chou, Appl. Phys. Lett. **81**, 3058 (2002).

[38] H. Cao, Z. Yu, J. Wang, J. O. Tegenfeldt, R. H. Austin, E. Chen, W. Wu, and S. Y. Chou, Appl. Phys. Lett. **81**, 174 (2002).

[39] A. Muralidhar, D. R. Tree, and K. D. Dorfman, Macromolecules **47**, 8446 (2014).

[40] L. Dai, J. Van Der Maarel, and P. S. Doyle, Macromolecules **47**, 2445 (2014).

[41] E. Werner and B. Mehlig, Phys. Rev. E **90**, 062602 (2014).

[42] Y. Yang, T. W. Burkhardt, and G. Gompper, Phys. Rev. E **76**, 011804 (2007).

[43] T. W. Burkhardt, Y. Yang, and G. Gompper, Phys. Rev. E **82**, 041801 (2010).

[44] T. Odijk, J. Polym. Sci. Polym. Phys. Ed. **15**, 477 (1977).

[45] J. Skolnick and M. Fixman, Macromolecules **10**, 944 (1977).

[46] A. V. Dobrynin, Macromolecules **38**, 9304 (2005).

[47] D. Stigter, Biopolymers **16**, 1435 (1977).

[48] A. Sischka, K. Toensing, R. Eckel, S. D. Wilking, N. Sewald, R. Ros, and D. Anselmetti, Biophys. J. **88**, 404 (2005).

[49] C. U. Murade, V. Subramaniam, C. Otto, and M. L. Bennink, Nucleic Acids Res. **38**, 3423 (2010).

[50] K. Günther, M. Mertig, and R. Seidel, Nucleic Acids Res. **38**, 6526 (2010).

[51] M. Reuter and D. T. F. Dryden, Biochem. Biophys. Res. Commun. **403**, 225 (2010).

[52] M. Maaloum, P. Muller, and S. Harlepp, Soft Matter **9**, 11233 (2013).

[53] N. Shi and V. M. Ugaz, Small **10**, 2553 (2014).

[54] B. Kundukad, J. Yan, and P. S. Doyle, Soft Matter **10**, 9721 (2014).

[55] T. T. Perkins, D. E. Smith, R. G. Larson, and S. Chu, Science **268**, 83 (1995).

[56] L. Nyberg, F. Persson, B. Åkerman, and F. Westerlund, Nucleic Acids Res. **41**, e184 (2013).

[57] S. M. Stavis, J. Geist, M. Gaitan, L. E. Locascio, and E. a. Strychalski, Lab Chip **12**, 1174 (2012).

[58] Y. Wang, D. R. Tree, and K. D. Dorfman, Macromolecules **44**, 6594 (2011).

[59] D. R. Tree, Y. Wang, and K. D. Dorfman, Phys. Rev. Lett. **110**, 208103 (2013).

[60] A. Muralidhar and K. D. Dorfman, Macromolecules **48**, 2829 (2015).

[61] P. Grassberger, Phys. Rev. E **56**, 3682 (1997).

[62] T. Prellberg and J. Krawczyk, Phys. Rev. Lett. **92**, 120602 (2004).

19

[63] D. R. Tree, A. Muralidhar, P. S. Doyle, and K. D. Dorfman, Macromolecules **46**, 8369 (2013).

[64] X. Li, C. M. Schroeder, and K. D. Dorfman, Soft Matter **11**, 5947 (2015).

[65] A. Muralidhar, D. R. Tree, Y. Wang, and K. D. Dorfman, J. Chem. Phys. **140**, 084905 (2014).

[66] S. S. Bahga, M. Bercovici, and J. G. Santiago, Computer Code Buffer Calculator, Stanford Microfluidics Laboratory, 2012. http://microfluidics.stanford.edu/download/.

[67] B. J. Kirby and E. F. Hasselbrink, Electrophoresis **25**, 203 (2004).

[68] J.-L. Viovy, Rev. Mod. Phys. **72**, 813 (2000).

[69] B. J. Kirby and E. F. Hasselbrink, Electrophoresis **25**, 187 (2004).

[70] R. Chang and K. Jo, J. Chem. Phys. **136**, 095101 (2012).

[71] C. Manneschi, P. Fanzio, T. Ala-Nissila, E. Angeli, L. Repetto, G. Firpo, and U. Valbusa, Biomicrofluidics **8**, 064121 (2014).

[72] O. Castillo-Fernandez, G. B. Salieb-Beugelaar, J. W. van Nieuwkasteele, J. G. Bomer, M. Arundell, J. Samitier, A. van den Berg, and J. C. T. Eijkel, Electrophoresis **32**, 2402 (2011).

[73] L. D. Menard and J. M. Ramsey, Nano Lett. **11**, 512 (2010).

[74] E. Werner and B. Mehlig, Phys. Rev. E **91**, 050601 (2015).